JOURNAL OF CATALYSIS 37, 486–502 (1975)

Surface, Catalytic and Magnetic Properties of Small Iron Particles

I. Preparation and Characterization of Samples

M. BOUDART,[1] A. DELBOUILLE, J. A. DUMESIC, S. KHAMMOUMA AND H. TOPSØE

Stauffer Laboratories of Chemistry and Chemical Engineering, Stanford University, Stanford, California 94305

Received October 3, 1974

Very small and stable metallic iron particles supported on magnesium oxide have been obtained in an average size d from 1.5 to 30 nm. The hydrogen reduced particles consist of metallic iron, magnesium oxide, and Fe^{2+} clusters in magnesium oxide. Values of d determined by electron microscopy, magnetic susceptibility, X-ray line-broadening and Mössbauer spectra agreed with those determined by selective chemisorption of carbon monoxide with a stoichiometry of two iron atoms per adsorbed molecule. As the iron loading was changed from 1 to 40 wt %, the fraction of the iron in the metallic state on the different reduced samples varied from 0.4 to 0.7, and the Fe^{2+} concentration in the Fe^{2+} clusters in magnesium oxide varied only little. These results, coupled with a study of the sample preparation, suggest that magnesium oxide is not merely an inert carrier for metallic iron, but instead interacts with the iron in a manner essential for the ultimate production and stabilization of small metallic particles.

INTRODUCTION

Many catalysts consist of small particles, and one of the problems in catalysis is the production and maintenance of small particle sizes and consequently high surface areas. In the case of metallic catalysts, this is often done by dispersing the metal on a porous support. Besides their practical importance, small metal particles have also recently attracted much attention as reactions have been found with turnover numbers which depend or not on the particle size of the metal, when the latter is varied between 1 and 10 nm (*1*). These reactions have been termed structure sensitive and insensitive, respectively, and it was suggested that the ammonia synthesis on iron is a structure sensitive reaction (*2*). Unfortunately no method of preparation of stable iron particles in the desired size range has been reported.

This paper is the first of a series where very small stable particles of metallic iron have been used to study the structure sensitivity of iron in ammonia synthesis and to identify the preferred sites for the reaction by means of kinetic, chemisorption and magnetic susceptibility measurements coupled with Mössbauer spectra. In this first paper, the preparation and structure of the samples used in subsequent papers, are described and discussed.

EXPERIMENTAL METHODS

Sample Preparation

Iron particles were supported on magnesium oxide by hydrogen reduction of a

[1] To whom queries should be addressed.

precursor which was prepared in the following manner. A slurry of 80 g of magnesium hydroxy-carbonate (Matheson, Coleman and Bell, magnesium carbonate basic powder) in 1.25 liters of doubly distilled water was stirred with a mechanical stirrer and heated to 340 K. Then 1.25 liters of an aqueous ferric nitrate (Baker and Adamson) solution preheated to 340 K were added rapidly to the slurry. The molality of the solution was the only variable changed in preparing catalysts with different iron loadings. After 0.5 hr of stirring at 340 K, the slurry was filtered, washed with doubly distilled water, and dried under vacuum at 360 K for 12 hr. Grinding of the precursor in a mortar completed the preparation procedure. Metal loading will be reported in wt% Fe referred to dry reduced sample, e.g., 5% Fe/MgO.

Carbon Monoxide Chemisorption

Carbon monoxide chemisorption was performed according to the ideas of Emmett and Brunauer (*3*) at 193 K with an apparatus described elsewhere (*4*). A known quantity of precursor was reduced in flowing, palladium-diffused hydrogen according to a reduction schedule which consisted of 2–5 hr at 370 K, 12–16 hr at 520 K, 2–5 hr at 600 K, 2–5 hr at 650 K, followed by at least 20 hr at 700 K. After the reduction, the sample was evacuated to 10^{-4} Pa for 3 hr at 670 K, cooled to 193 K, and a CO isotherm was taken. Evacuation to 10^{-3} Pa for 0.5 hr at 193 K followed the first isotherm, and a second isotherm was then recorded. The CO (99.5%) was purified by slow passage through a molecular sieve trap at 193 K. Volumetric oxidation experiments on reduced samples were performed on the same adsorption apparatus.

Mössbauer Spectroscopy

Mössbauer spectra were taken using the spectrometer described elsewhere (*5*). The source was 100 mCi of ^{57}Co diffused into Cu. Absolute velocities were determined by means of an Austin Science Associates helium laser interferometer.

A known amount of sample (ca. 0.3 g) was compressed into a 1.9 cm diameter wafer and was loaded into a vacuum cell made of quartz to obtain Mössbauer specta between 300 and 870 K, the temperature being controlled to within ±1 K by a temperature controller (Gulton Model JAD) and a thermocouple located near the sample. The cell was connected to a multipurpose gas handling vacuum system which allowed evacuation to pressures of 10^{-4} Pa, and flowing of H_2, He, O_2, and a $H_2:N_2$ mixture at atmospheric pressure. For purification purposes, the H_2 was passed through a palladium–silver thimble (Milton Roy), the He was passed through a column of copper turnings at 470 K and then through a molecular sieve (Linde Corp. 13X) trap at liquid nitrogen temperature, the O_2 was flowed through a similar molecular sieve trap at 193 K, and the $H_2:N_2$ mixture was passed through a Deoxo hydrogen purifier and then through a molecular sieve trap at 193 K.

X-Ray Diffraction

A Picker biplanar diffractometer was used with both Cu $K\alpha$ and Mo $K\alpha$ radiations (scintillation and solid-state detectors, respectively). Some samples were first reduced according to the reduction schedule described above, and then passivated by flowing He (99.9%) over each sample at room temperature, followed by the slow admittance of air to the reduction cell. Other samples were reduced in a special two-section cell which enabled X-ray spectra to be obtained in H_2. Reduction of the sample, in wafer form, was performed in one section of the cell, and diffraction spectra were obtained after transport of the wafer to the other section of the cell equipped with Mylar windows. A polycrystalline quartz sample was used to cor-

rect for instrumental broadening in particle size determinations. Ground Si single crystals were mixed with the sample when accurate structural parameters were sought.

Magnetic Susceptibility Balance

Magnetic susceptibility data were obtained by the Faraday method. A water-cooled electromagnet provided variable fields up to 300 kA m^{-1} and field gradients up to 3 MA m^{-2}. The sample was suspended in a quartz bucket from a Cahn electrobalance enclosed in a vacuum system, and magnetic data could be obtained in static H_2, He, $H_2:N_2$ or in a vacuum of 10^{-4} Pa at temperatures between 77 and 720 K. The H_2 was purified by passage through a Deoxo unit and then through a molecular sieve trap at liquid nitrogen temperature. The He and the $H_2:N_2$ mixture were purified as described above.

RESULTS

Mössbauer Spectroscopy

Mössbauer spectra of fully reduced samples (Fig. 1) under flowing H_2 at 298 K indicate two forms of iron. The first form of iron gives rise to the magnetically split six-peak spectral component (five of the peaks are visible, with the sixth peak hidden in the central region of the spectrum), and by comparison with the spectrum of a metallic iron foil at 298 K (Fig. 1), the first form of iron can be identified as metallic iron. The second form of iron is responsible for the spectral doublet in the central region of the spectrum.

A computer analysis of the γ-ray data was made with a version of the Argonne variable metric minimization program to fit Lorentzian line shapes. To obtain a physically meaningful fit of the data, the following constraints were imposed. The dip and width of the hidden peak from the magnetically split component were constrained to be equal to the dip and width of the third peak counting from left to right in Fig. 1. The position of this hidden peak was constrained to the value calculable from the visible peaks. Equality of the dips and widths of the two peaks forming the central doublet was also contrained in the final fit of the data. As there is a shoulder on the low-velocity side of the left peak of the central doublet, one unconstrained peak was assigned to this spectral component in the final fit.

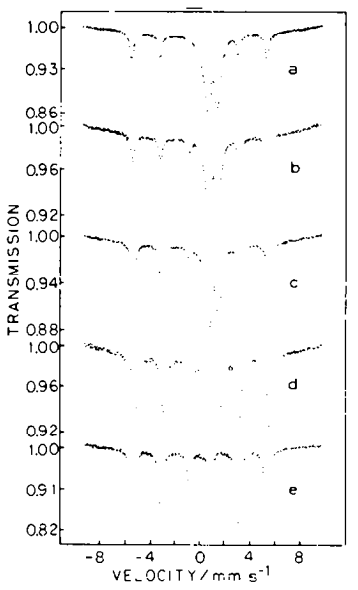

FIG. 1. Mössbauer spectra at 298 K of reduced Fe/MgO samples: (a) 1% Fe/MgO; (b) 5% Fe/MgO; (c) 16% Fe/MgO; (d) 40% Fe/MgO; (e) NBS Fe foil.

The results of the computer analysis are summarized in Table 1. The isomer shift of the central doublet indicates that one form of iron is Fe^{2+} (*6–9*). The equality of the magnetic field and the isomer shift for the magnetically split spectral component to the corresponding parameters for metallic iron confirms the assignment of metallic iron to the magnetically split spectral component (*10*).

By taking the ratio of the area corresponding to the metallic iron to the total spectral area at room temperature, the fraction of the iron in the metallic state

TABLE 1
MÖSSBAUER PARAMETERS FOR REDUCED Fe/MgO SAMPLES AT 298 K

Parameters	Fe/MgO 1%	Fe/MgO 5%	Fe/MgO 16%	Fe/MgO 40%	Fe foil
T (K)	298	298	298	298	298
Magnetically split spectral area A_{hfs} (mm s^{-1})	0.12	0.073	0.18	0.21	—
Fe^{2+} spectral area $A_{Fe^{2+}}$ (mm s^{-1})	0.23	0.13	0.19	0.088	—
Central peak area A_{cp} (mm s^{-1})	0.030	0.0070	0.0068	0.014	—
$\frac{A_{hfs} + A_{cp}}{A_{hfs} + A_{cp} + A_{Fe^{2+}}}$	0.39	0.38	0.49	0.72	—
$\frac{A_{cp}}{A_{hfs} + A_{cp}}$	0.20	0.10	0.04	0.05	—
Metallic isomer shift[a] δ (mm s^{-1})	0.000	−0.005	0.000	0.001	0.000
Magnetic field H (MA m^{-1})	26.26	26.30	26.29	26.37	26.19
Fe^{2+} isomer shift δ (mm s^{-1})	1.043	1.047	1.045	1.053	—
Fe^{2+} quadrupole splitting E_Q (mm s^{-1})	0.802	0.792	0.817	0.810	—
Central peak isomer shift δ (mm s^{-1})	0.07	0.08	0.30	−0.71	—

[a] All isomer shifts reported with respect to metallic iron at 298 K.

can be estimated, for similar recoil-free fractions of the metal and the oxide. The fraction of metallic iron can also be determined by measuring the saturation magnetization of the reduced sample, or by measuring at 620 K the uptake of oxygen by the reduced sample. The latter determination is based on the fact that all of the iron (metallic and Fe^{2+}) is oxidized to Fe^{3+} at 620 K in oxygen, as determined by Mössbauer spectroscopy (Fig. 3). The agreement for the value of the fraction of metallic iron as determined by Mössbauer spectroscopy with that obtained by magnetic susceptibility and volumetric oxidation (Table 3) shows that the room temperature spectral area ratio is a good measure of the fraction of metallic iron in the various reduced samples.

In Fig. 2 are shown Mössbauer spectra, taken at 683 K under flowing H_2, of the same samples which were used in Fig. 1, and the results of a computer analysis of these spectra are summarized in Table 2. When the small iron particles are converted to γ-Fe_2O_3 by a 490 K treatment in flowing O_2, dramatic changes in the Mössbauer spectra with temperature are observed (Figs. 3 and 4). Further treatment at 620 K in O_2 transformed the larger particles to α-Fe_2O_3 (Fig. 5).

Besides Mössbauer spectra taken on completely reduced samples, spectra were also taken at various stages of the initial reduction. The spectra, for 1% Fe/MgO are shown in Fig. 6. From these spectra, it can be seen that the iron in the unreduced precursor is present as Fe^{3+}, which is reduced to Fe^{2+} near 540 K, and the final fraction of metallic iron is attained at ca.

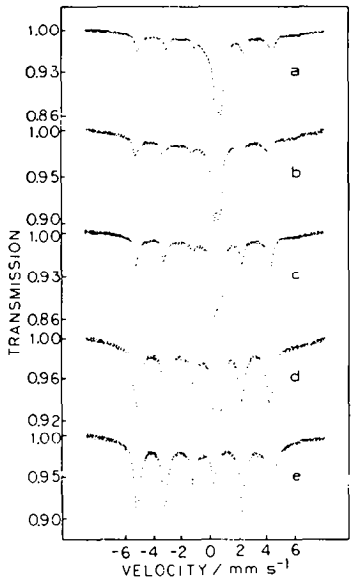

FIG. 2. Mössbauer spectra at 673 K of reduced Fe/MgO samples: (a) 1% Fe/MgO; (b) 5% Fe/MgO; (c) 16% Fe/MgO; (d) 40% Fe/MgO; (e) NBS Fe foil.

620 K. (The spectral parameters of Fe^{3+} and Fe^{2+} are discussed below.)

Carbon Monoxide Chemisorption

In Fig. 7 are shown the pair of CO isotherms obtained as described earlier on the 5% Fe/MgO reduced sample. They are displaced by a constant CO uptake, corresponding to the amount of strongly adsorbed CO, as shown for this and other samples in Table 3. A 8% Fe/MgO reduced sample subsequently reoxidized in O_2 at 298 K did not strongly adsorb Co. Thus, the chemisorption of CO on the support, MgO, and on Fe^{3+} can be ruled out, leaving the metallic iron and possibly Fe^{2+} as CO chemisorbents. From the assumed

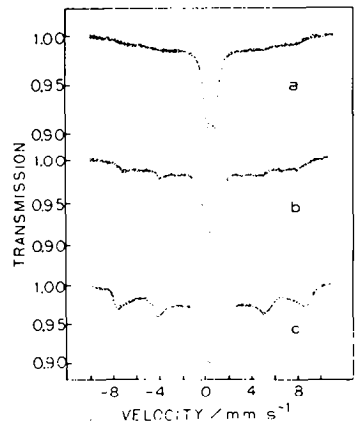

FIG. 3. Mössbauer spectra of γ-Fe_2O_3 in 5% Fe/MgO: (a) 298 K; (b) 200 K; (c) 77 K.

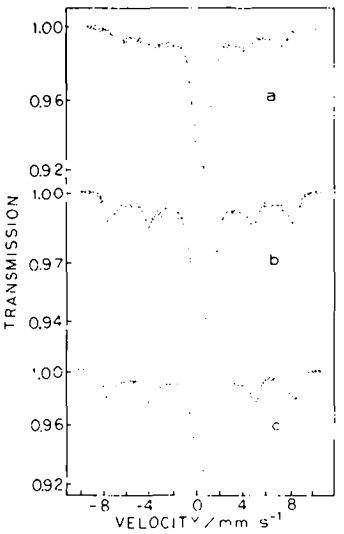

FIG. 4. Mössbauer spectra of γ-Fe_2O_3 in 12% Fe/MgO: (a) 490 K; (b) 298 K; (c) 195 K.

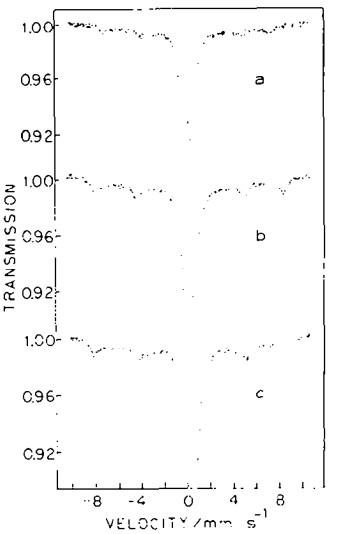

FIG. 5. Mössbauer spectra of α-Fe_2O_3 in 12% Fe/MgO: (a) 595 K; (b) 298 K; (c) 195 K.

TABLE 2
MÖSSBAUER PARAMETERS FOR REDUCED Fe/MgO SAMPLES AT 673 K

Parameters	Fe/MgO 1%	5%	16%	40%	Fe foil
T (K)	673	673	673	685	673
Magnetically split spectral area A_{hfs} (mm s^{-1})	0.076	0.047	0.12	0.18	—
Fe^{2+} spectral area $A_{Fe^{2+}}$ (mm s^{-1})	0.14	0.079	0.13	0.055	—
Central peak area A_{cp} (mm s^{-1})	0.032	0.016	0.011	0.0014	—
$\frac{A_{hfs} + A_{cp}}{A_{hfs} + A_{cp} + A_{Fe^{2+}}}$	0.44	0.44	0.52	0.77	—
$\frac{A_{cp}}{A_{hfs} + A_{cp}}$	0.30	0.25	0.08	0.01	—
Metallic isomer shift[a] δ (mm s^{-1})	−0.241	−0.243	−0.240	−0.251	0.240
Magnetic field H (MA m^{-1})	23.12	23.17	23.21	22.97	23.21
Fe^{2+} isomer shift δ (mm s^{-1})	0.786	0.783	0.786	0.799	—
Fe^{2+} quadrupole splitting E_Q (mm s^{-1})	0.375	0.389	0.385	0.799	—
Central peak isomer shift δ (mm s^{-1})	−0.05	−0.38	−0.83	−0.41	—

[a] All isomer shifts reported with respect to metallic iron at 298 K.

Fe:CO = 2:1 surface stoichiometry (*11*) and the fractional metallic iron obtained from Mössbauer spectroscopy, the metallic iron dispersion, D (the fraction of the metallic iron atoms that are surface atoms), can be calculated. The particle size, d, is then obtained using the relation that d (nm) = C/D with $C = 0.85$ (*12*). Alternatively, the metallic iron particle size can be calculated assuming a spherical

TABLE 3
REDUCED Fe/MgO GENERAL CHARACTERIZATION

Sample % Fe/MgO	Measured wt% Fe[a]	Fraction of iron in metallic state: Mössbauer spectroscopy	Magnetic susceptibility	Volumetric oxidation	CO uptake[a] (μmol g^{-1})
1	0.95	0.39	0.50	0.35	18
5	4.9	0.39	—	—	41
8	8.1	—	0.55	—	—
12	12	0.47	—	—	—
16	17	0.49	—	—	58
40	37	0.72	—	—	67

[a] All weights reported on a dry, reduced basis.

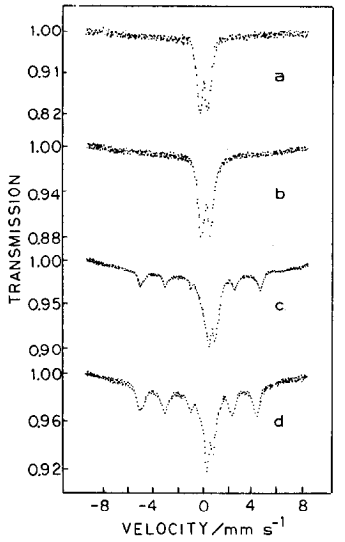

FIG. 6. Mössbauer spectra of reduction process of 1% Fe/MgO: (a) 298 K; (b) 480 K; (c) 550 K; (d) 620 K.

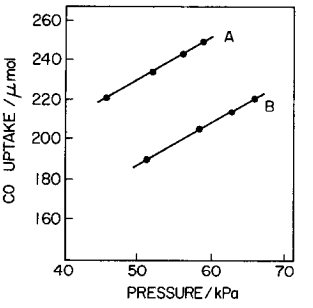

FIG. 7. Carbon monoxide isotherms at 193 K on 5% Fe/MgO: (A) first isotherm; (B) second isotherm.

shape using the cross-sectional area of a CO molecule (0.135 nm²) (*13*), and both methods give particle sizes which agree with each other within the experimental uncertainty. In Table 4 are summarized the surface average metallic iron particle sizes for various samples determined using the 2:1 Fe:CO stoichiometry.

X-Ray Diffraction

In Fig. 8 is shown a section of the X-ray diffraction pattern, using Cu radiation, of the passivated 16% Fe/MgO sample. At the highest value of 2θ is the metallic iron peak ($hkl = 110$). The position of the metallic iron diffraction peak was, within experimental error, independent of the metallic iron particle size for all of the samples except 1% Fe/MgO, on which no

TABLE 4
REDUCED Fe/MgO METALLIC IRON PARTICLE SIZE CHARACTERIZATION

		Metallic iron particle size (nm)					
		CO chemisorption	X-Ray line-broadening	Magnetic susceptibility (V: particle vol)		Electron microscopy	
% Fe/MgO	Dispersion: CO chemisorption	Surface av	Vol av	$\langle V \rangle^{1/3}$	$\left[\frac{\langle V^2 \rangle}{\langle V \rangle}\right]^{1/3}$	Surface av	Vol av
1	0.53	1.5	No visible iron peak	3.5	5.0	—	
5	0.23	4.0	7.0	—		4.5	5.5
8	—	—	9.0	4.5	6.5	—	
12	—	—	11	—		11	13
16	0.078	10	14	—		—	
40	0.028	30	42	—		—	

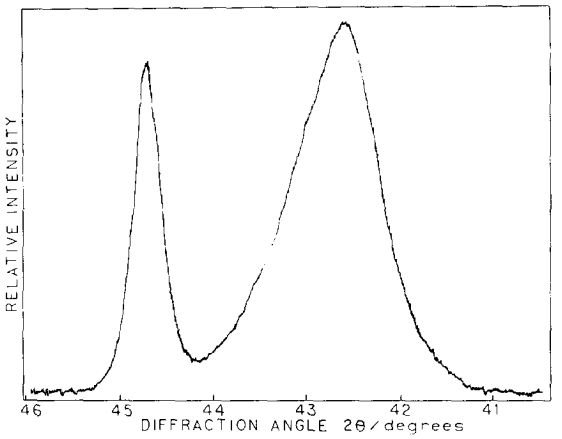

FIG. 8. X-Ray diffraction scan of 16% Fe/MgO.

metallic iron peak could be resolved. Thus, no lattice expansions or contractions were observed for the small iron particles supported on MgO.

It is clear from Fig. 8 that the diffraction peak appearing to the right of the metallic iron peak is asymmetric to the high-angle side. This asymmetric peak can roughly be resolved into two symmetric peaks, one at 42.8° and the other at 42.4° in 2θ. The position of the first broad peak agrees well with that for small particles of MgO (as determined for a sample which did not contain iron) and the second peak corresponds to a solid solution of FeO–MgO with a composition of about 40% atomic FeO, using a linear relation between lattice parameter and at.% FeO in MgO. Clearly, the reduced sample is a three-phase system of metallic iron, MgO, and FeO–MgO.

The metallic iron particle size was calculated for passivated samples using the Scherrer equation correcting for both instrumental broadening using Warren's correction (*14*), and the $K_{\alpha 1}$ and $K_{\alpha 2}$ doublet (*15*). Mo radiation was found most convenient for these determinations; in all possible cases both the (110) and (211) diffractions were used, and for the larger iron particles the (200) diffraction was also used in particle size determinations. Large anisotropies in the shape of metallic iron particles were not observed for any of the samples, and the volume average metallic iron particle sizes for the various samples are collected in Table 4. X-Ray scans were also made on some samples under H_2 in the cell enabling direct measurements on the reduced samples. The particle sizes of the iron crystals obtained in this way agreed with those listed in Table 4 within experimental error. This indicates that the passivation of the iron particles only affects a small fraction of the metallic iron atoms, which was verified by Mössbauer spectroscopy, where the area decrease of the metallic iron peaks was less than 15% upon passivation of samples with iron loadings greater than or equal to 5%.

From the broadening of the MgO peaks in the spectra of the different samples, the MgO volume average particle size was observed to increase progressively from 5.5 to 6.5 nm upon increasing the loading of iron from 1 to 16%. No shape anisotropy was detected by studying the (200), (220), and (222) diffractions. The particle size of the FeO–MgO phase, for the 16% and 40% Fe/MgO samples, where the peaks could be resolved, was found to be roughly the same as that of the metallic iron phase on the same sample.

An X-ray diffraction scan of a sample of vacuum-decomposed, pure magnesium hy-

droxy-carbonate showed that the decomposition produced MgO particles 5.0 nm in size. Thus, it appears that the presence of iron slightly increases the MgO particle size, in agreement with the results of Guilliatt and Brett (*16*). In addition, the lattice parameter for the MgO particles was 0.5% larger than that for bulk MgO, indicating a lattice expansion for the small MgO particles. This has also been observed by Anderson (*17*). X-Ray diffraction was also performed on unreduced precursors, and these results will be discussed later.

Magnetic Susceptibility

The magnetization, M, as a function of temperature, T, and applied field, H, was measured for the 1% Fe/MgO and 8% Fe/MgO samples. The detailed results are given elsewhere (*18*). From the saturation magnetization of each sample, the fraction of metallic iron for 1% Fe/MgO and 8% Fe/MgO was found to be 0.50 ± 0.05 and 0.55 ± 0.05, respectively. Above a certain temperature, $\bar{T}_B$, when M was plotted against H/T, the data for different temperatures could be fitted on a single curve indicating superparamagnetic behavior (*19*). For 1% Fe/MgO, $\bar{T}_B$ was about 190 K, and for 8% Fe/MgO, $\bar{T}_B$ was about 350 K. Below $\bar{T}_B$, substantial deviations from superparamagnetic behavior were observed.

From the shape of the M versus H/T curves above $\bar{T}_B$, the metallic iron particle size can be calculated, since Fe^{2+} contributes only to a negligible extent to the measured magnetization (*20*). The high field data give the average particle volume $\langle V \rangle$ and the low field data give the average of the squared volume divided by the average volume, $\langle V^2 \rangle / \langle V \rangle$. Appropriate average particle sizes were obtained by taking the cube root of the respective volume averages, and the particle sizes so obtained are listed in Table 4.

Electron Microscopy

During the preparation and reduction of the samples, a number of chemical processes occur, and the effect of each process on the ultimate nature of the sample is not at all clear. To understand the catalyst genesis more completely, electron microscopy was employed at several stages of preparation.

An electron micrograph of the magnesium hydroxy-carbonate powder at 23,000× magnification is shown in Fig. 9, and it can be seen that the particles of the hydroxy-carbonate are plate-like, with many of the plates having regular symmetry. The characteristic dimension of these two-dimensional plates is about 300 nm and the BET surface area was measured to be 20 $m^2\ g^{-1}$. Correspondingly, the thickness of the plates must be about 20 nm.

After preparation of the 5% Fe/MgO precursor, an electron micrograph of the latter at 23,000× magnification was taken (Fig. 9). The plate-like structure of the hydroxy-carbonate is preserved, but the regular symmetry seems to have been partially destroyed, and the characteristic dimension of the plates has decreased to about 100 nm. The precursor was then reduced according to the reduction schedule, and after passivation at room temperature another electron micrograph was taken at 23,000× magnification (Fig. 9). The original shape of the hydroxy-carbonate particles is still evident, but each of the large 100 nm plates is a collection of smaller particles with a characteristic dimension of about 5 nm. It is known that magnesium hydroxide and magnesium carbonate decompose to magnesium oxide at temperatures of about 620 K (*21*), and thus the small 5 nm particles which are grouped together into plate-like structures are magnesium oxide particles (*22*). Also present in the electron micrograph are small particles of iron which appear as dark (almost black) spots. The characteristic size of these particles is also about 5 nm. The BET surface area of a decomposed hydroxy-carbonate sample was 280 m^2/g of magnesium oxide formed, corre-

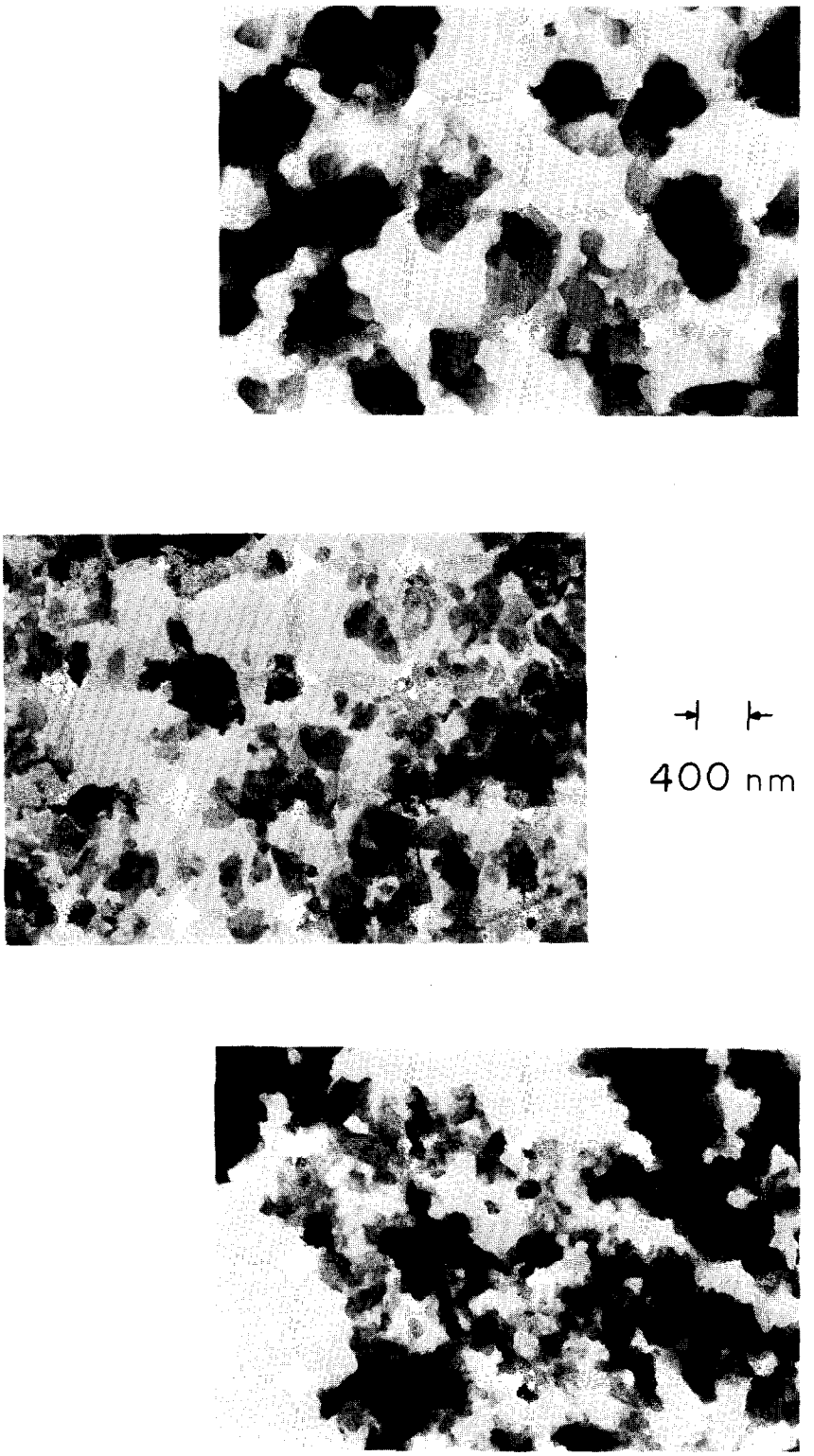

FIG. 9. Electron micrographs at 23,000× magnification of 5% Fe/MgO genesis: (top) magnesium hydroxycarbonate; (middle) precursor; (bottom) reduced sample.

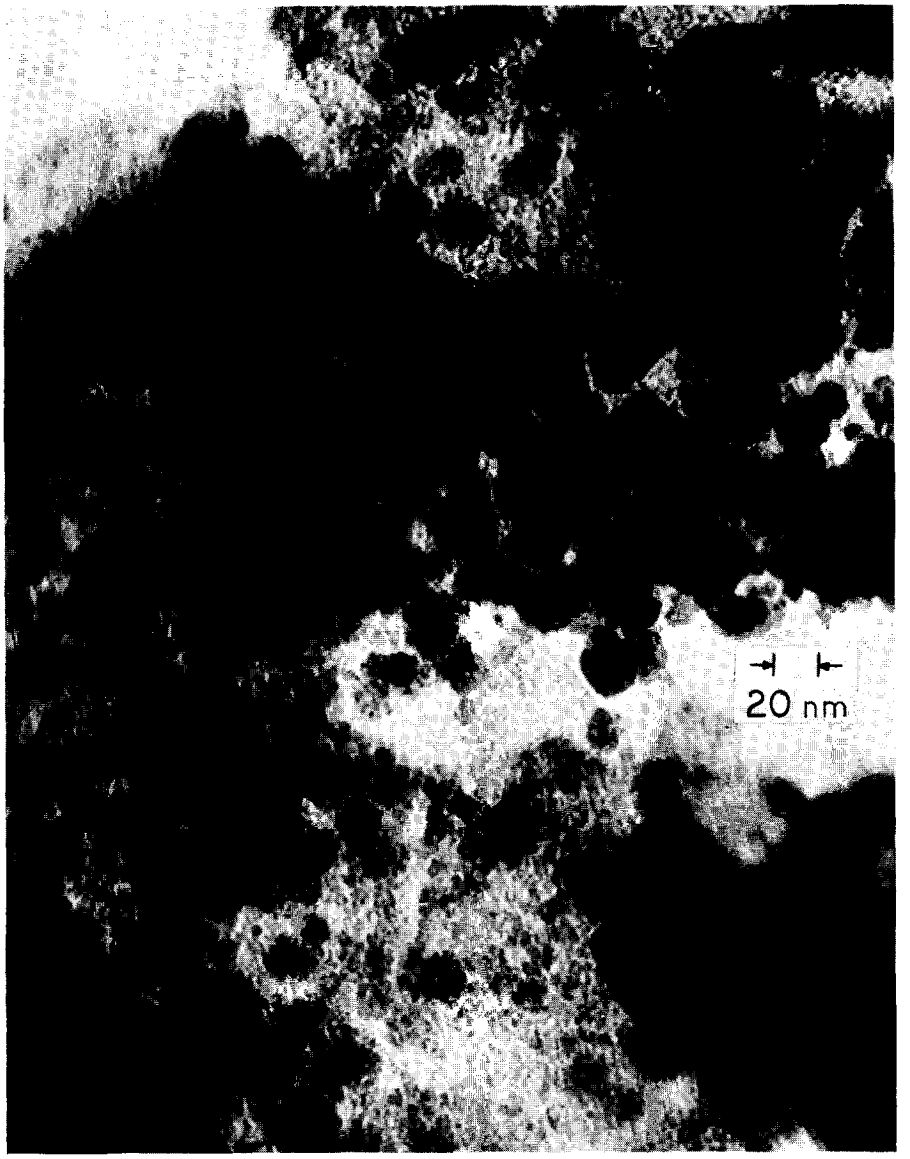

FIG. 10. Electron micrograph at 500,000× magnification of reduced 5% Fe/MgO.

sponding to a magnesium oxide particle size of 6 nm. Both of these results are in agreement with the X-ray results mentioned above.

To study the small iron particles in greater detail, electron micrographs of the passivated 5% Fe/MgO sample were taken at a magnification of 500,000 times (Fig. 10). The iron particles again appear as dark spots on the micrograph. From a sampling of 160 iron particles, the iron particle size distribution was estimated, and the volume average and surface average metallic iron particle sizes, calculated from this distribution, are listed in Table 4. The results of a similar analysis of 12% Fe/MgO are also given in Table 4.

DISCUSSION

Particle Size Comparisons

For the determination of turnover numbers in reactions over supported metals,

the number of surface metallic atoms must be known. This is directly obtained by selective chemisorption, once the gas–metal stoichiometry is known. However, such measurements provide no information about shape and size distribution, which must be obtained by other physical measurements. The latter may also yield information about possible changes in adsorption stoichiometry as particle size is decreased.

The first interesting result of this study is that small iron particles have been produced with sizes ranging from about 1.5 to 30 nm. Furthermore, these particles show very little tendency to sinter in either hydrogen or under conditions of ammonia synthesis (*23*).

The metallic iron particle size was determined in various ways. X-Ray line-broadening proved to be a useful technique for studying the metallic iron particles on the 8, 12, 16, and 40% Fe/MgO samples. The X-ray diffraction studies also showed the absence of large anisotropies in particle shape. Magnetic susceptibility measurements on 1% Fe/MgO and electron microscopy on 5% Fe/MgO were the additional tools used to complete the particle size characterization. The good agreement between the results of the X-ray line-broadening and the magnetic susceptibility on 8% Fe/MgO, and the X-ray line-broadening and the electron microscopy on 12% Fe/MgO gives credibility to the overall characterization of the samples.

For the study of catalytic processes over the metallic iron particles supported on MgO, the metallic iron surface area (or a quantity proportional to it) must be known for the various catalysts. However, the average particle size, as determined by any of the above techniques, does not yield the metallic iron surface area directly. The fraction of metallic iron, the total iron loading, and the relation between particle size and surface area must be known. The first two requirements involve additional experimental measurements and the relation between particle size and surface area can only be approximated.

On the other hand, the CO chemisorption results give the number of metallic iron surface atoms directly. The dispersion of the metal can be obtained from the amount chemisorbed, the fraction of metallic iron, and the total iron loading. Finally, from the relation between dispersion and particle size, the latter can be calculated. The agreement between the value of the metallic iron particle size measured directly, using methods discussed earlier, and that calculated from the CO chemisorption is excellent, especially when the averaging processes inherent in the different measurements are considered. It can therefore be concluded that the CO chemisorption technique, with the aforementioned stoichiometry, is applicable to the present system with iron particle sizes down to at least 1.5 nm. Finally, let us note that our Fe/MgO system contrasts with previously discussed small iron particle systems, where the iron was completely surrounded by the supporting matrices (*24,25*). In our system, the iron surface is accessible to gases and therefore can be used in catalysis.

Mössbauer Spectroscopy

As mentioned earlier, dramatic changes in the Mössbauer spectra of the oxidized samples are produced by varying the temperature at which the spectra are taken, and these changes can be attributed to superparamagnetic behavior. If the anisotropy energy barrier for the spin flipping is known, an average particle size for the magnetic phase can be estimated knowing the temperature at which 50% of the magnetic phase is superparamagnetic, T_B (*26*). Specifically, the particle size dependent magnetic relaxation frequency at T_B is set equal to the Larmor precession frequency of the nuclear moment about the internal magnetic field. For each spectrum of Fig. 5, the fraction of the magnetic phase behaving superparamagnetically can be

graphically determined, and the temperature dependence of this fraction allows the estimate $T_B = 400$ K to be made. For α-Fe_2O_3, the anisotropy energy barrier has been determined for particles in the 10 nm range (*27*), and from this value (8×10^{-3} J cm^{-3}), coupled with the value of T_B for 12% Fe/MgO, the average particle size of 14 nm of α-Fe_2O_3 for this sample was calculated. This corresponds to an average metallic iron size of 12 nm, in good agreement with the other determinations. When the Fe/MgO samples were oxidized, γ-Fe_2O_3 showed to be a quite stable product. The γ-oxide particles obtained by oxidizing both 12 and 5% Fe/MgO exhibited superparamagnetic behavior. The values for the anisotropy energy barriers of 3×10^{-2} and 8×10^{-2} J cm^{-3} were obtained using 12 and 6 nm for the respective average metallic diameters. These values are much larger than that value based on crystalline anisotropy (*28*) and must originate from other forms of anisotropy, as expected in view of the ferrimagnetic behavior of γ-Fe_2O_3. Indeed, the above anisotropy energy barriers for the γ-oxides are not unreasonably large, in view of the 1.2×10^{-1} J cm^{-3} anisotropy barrier observed by Coey and Khalafalla (*29*) for γ-Fe_2O_3 particles in the 10 nm range.

The Mössbauer parameters of the Fe^{3+} doublet present in the spectra of the oxidized samples are those of Fe^{3+} in MgO. The 298 K isomer shift (all isomer shifts are with respect to metallic iron at 298 K), independent of metal loading, is 0.35 mm s^{-1}, which is within the experimental uncertainty of 0.37, 0.38, and 0.36 mm s^{-1} obtained by others for metal loadings in MgO of 325 ppm, 0.5 and 6.5 at.%, respectively (*8,6,30*). The 298 K quadrupole splitting decreases slightly from 0.63 mm s^{-1} for 5% Fe/MgO to 0.58 mm s^{-1} for 12% Fe/MgO. These values parallel quite nicely the literature values of 0.82, 0.70, and 0.66 mm s^{-1} for Fe^{3+} loadings in MgO of 325 ppm, 0.5 and 6.5 at.%, respectively (*8,6,30*). Yet, the Fe^{3+} in MgO data at 298 K may be complicated by the superparamagnetic behavior of the α-Fe_2O_3, since it is known that the quadrupole splitting of superparamagnetic α-Fe_2O_3 increases as the oxide particle size decreases (*27*). However, the same trends in the Mössbauer parameters of the Fe^{3+} doublet (independence of the isomer shift and increase in the quadrupole splitting with respect to decrease in metal loading) are seen at 77 K, a temperature at which superparamagnetic effects can be neglected in the present cases.

The Mössbauer parameters of the Fe^{2+} doublet present in the spectra of the reduced samples are also those of Fe^{2+} in MgO. The room temperature isomer shift (Table 1) is independent of metal loading, and is in excellent agreement with literature values of the Fe^{2+} in MgO isomer shift which is independent of metal loading from about 1 to 75 at.% (*9,7*). In contrast to the behavior of Fe^{3+}, however, the quadrupole splitting of the Fe^{2+} in MgO doublet is concentration dependent over a certain metal loading range. For loadings in MgO less than about 6 at.% no 298 K quadrupole splitting is observed (*9,6*). The quadrupole splitting increases to 0.30 mm s^{-1} for 8 at.% iron in MgO (*8*), and for metal loadings greater than 10 at.% in MgO the splitting is fairly constant and is 0.68 mm s^{-1} (*7*).

Clearly, in agreement with the X-ray diffraction results, the Fe^{2+} is not randomly distributed throughout the MgO. In fact, for the 1% Fe/MgO samples the quadrupole splitting of the Fe^{2+} doublet indicates that the local environment of the Fe^{2+} ions is at least 20 times more concentrated in iron than would be expected for random distribution. Thus, an FeO–MgO phase must be present along with a metallic iron and a MgO phase.

While the Mössbauer spectra of the oxidized samples show the presence of small oxide particles, the Mössbauer spectra of

the metallic iron in the reduced samples do not readily indicate superparamagnetic behavior. Furthermore, the hyperfine parameters do not appear to change as the particle size of the metal is decreased. The relation between metallic iron particle size and Mössbauer spectral behavior is, therefore, more subtle than in the oxide case. This must be due to the presence of a large anisotropy energy barrier for the metallic iron particles.

Unlike the oxides, where the particle magnetizations are small due to partial antiparallel spin alignments, the particle magnetization for metallic iron is quite large. Thus, demagnetization effects are more important for the metal than for the oxides, and for this reason the shape anisotropy energy barrier will be much larger for the former than for the latter. Although X-ray diffraction and electron microscopy show no large anisotropies in particle shape, aspect ratios of about 0.5 are still consistent with the data. A reasonable value for the shape anisotropy energy constant for metallic iron then, with an aspect ratio of 0.5, is about 1 J cm^{-3} (*31*). To calculate the metallic iron anisotropy energy constant from the Mössbauer data, the temperature at which 50% of the metallic iron is superparamagnetic must be estimated, and in order to do this, more must be said about the spectral component giving rise to the shoulder on the low-velocity side of the left peak of the Fe^{2+} doublet.

The computer estimate of the isomer shift of this peak for the 1 and 5% Fe/MgO samples is, within the rather large uncertainties (± 0.15 mm s^{-1}) involved in fitting this region, equal to that of metallic iron. That the unknown peak is not due to the left peak of a Fe^{3+} doublet is illustrated in the temperature dependence of the spectral area of this peak. For both the 1 and 5% Fe/MgO samples, the area of the unknown peak increases with respect to the area of the hyperfine split metallic iron when the temperature is increased. Since it is not reasonable to assert that the formation of Fe^{3+} is favored at higher temperatures in H_2, the area of the unknown peak would have decreased with respect to the metallic iron spectral area upon temperature increase due to the smaller recoil-free fraction of Fe^{3+} than that of metallic iron. For the 16 and 40% Fe/MgO samples, the area of the unknown peak was less than 5% of the metallic iron spectral area, and the position of this peak was incompatible with that of metallic iron. Clearly, in these two samples, very little superparamagnetic metallic iron is present.

From the computer estimate of the amount of superparamagnetic metallic iron for the 1% Fe/MgO sample as a function of temperature (Tables 1 and 2), the temperature at which 50% of the metallic iron is superparamagnetic can be estimated to be approximately 770 K. This temperature coupled with a volume average particle size of 2.5 nm gives rise to an anisotropy energy barrier of about 1 J cm^{-3}. Thus, the Mössbauer spectra of the reduced samples are indeed those expected for small particles. The magnetic properties of these small metallic iron particles will be discussed in greater detail in a subsequent paper (*32*).

Genesis of the Supported Metal Samples

Stable small iron particles result after reduction of the Fe/MgO precursors. Furthermore, over a 40-fold change in iron loading the fraction of the iron reduced to metallic iron stays almost constant. This behavior is quite different from that of other metal–oxide systems (*33–35*) and in order to understand the present system, the structure of the unreduced and reduced samples will be discussed. The magnesium hydroxy-carbonate used as a starting material in the catalyst preparation showed the positions and relative intensities of the X-ray diffraction peaks reported for $Mg_4(OH)_2(CO_3)_3 \cdot 3H_2O$ (*36*), which was

the sole phase, as confirmed by chemical analysis for Mg, C, O and H. The unreduced 1% Fe/MgO precursor showed an identical X-ray diffraction pattern to that of the magnesium hydroxy-carbonate, with no observable diffractions due to iron. It can thus be said that in making the Fe/MgO precursors, the structure of the starting material is preserved prior to reduction. When the metal loading was increasing (5, 16, 40% Fe/MgO), the qualitative features of the magnesium hydroxy-carbonate spectrum remained unchanged. Of more direct value, however, was the appearance of a new phase when the metal loading was increased, the intensity of the diffractions from this phase increasing with metal loading.

Three new diffractions of approximately equal intensity appear upon increasing metal loading to 5%. Their lattice parameters are 0.797, 0.400, and 0.264 nm. The same pattern was also obtained when solutions containing both ferric nitrate and magnesium nitrate were precipitated using NaOH under conditions similar to the precursor preparation. These peaks cannot be assigned to compounds which can be made by precipitation of Fe^{3+} by OH^- in aqueous solution. Ferric nitrate solutions, of the same molality as those used in the precursor preparation, were then precipitated using NaOH under conditions similar to the catalyst preparation. The precipitates were filtered and dried under vacuum at 360 K. Important variables in this procedure were the pH and temperature at which precipitation was initiated. In all cases, either γ-FeOOH (pH = 3; T = 345 K), α-FeOOH (pH = 6; T = 345 K), or a mixture of γ-FeOOH and α-FeOOH (pH = 6; T = 298 K) were obtained as revealed by their known X-ray diffraction patterns (*37,38*). Thus, in the unreduced precursor, a phase or interface is present which contains both Mg^{2+} and Fe^{3+}. The magnesium hydroxy-carbonate, therefore, does not merely act as a support for precipitated iron, but instead forms a two- or three-dimensional phase with it.

After complete reduction, electron micrographs show that the distribution of iron over the MgO is not homogeneous. In general, surrounding each dark contrast region (metallic iron) is a region of medium contrast, and this region is probably an area of high Fe^{2+} concentration. Indeed, it is well known that Fe^{2+} in MgO is not homogeneously distributed, but instead tends to form Fe^{2+} clusters in the MgO structure (*20*), and this is confirmed in the present study by the presence of X-ray diffraction peaks characteristic of both MgO and FeO–MgO. From the width of the FeO–MgO peak, the particle size of the FeO–MgO phase was greater than or equal to that of the metallic iron particle size. From the position of the FeO–MgO peak, the concentration of iron in the FeO–MgO phase was only a weak function of the total iron loading (less than proportional). This latter result is consistent with the independence of the Fe^{2+} quadrupole splitting over a 40-fold change in the total iron loading. Thus, Fe^{2+} clusters of roughly the same iron concentration are present in the different Fe/MgO samples. The concepts discussed above are schematically illustrated in Fig. 11.

The production of small metallic iron particles using MgO as a support may be understood in terms of the various iron and magnesium containing compounds encountered in the genesis of the reduced sample. Without the presence of a strong iron–support interaction, it seems likely that small metallic iron particles could not have been produced due to the well-known tendency of metallic iron to sinter (*39*). Yet, too strong an interaction between the iron and support suppresses the reduction of Fe^{2+} to metallic iron for low metal loadings (*35*). The nature of the FeO–MgO interaction, however, clusters the Fe^{2+}, thereby isolating the resulting metallic iron particles formed upon further

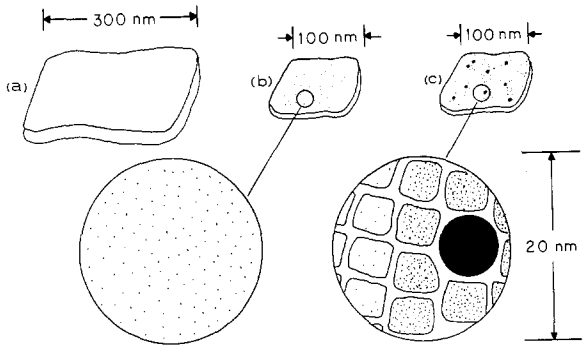

FIG. 11. Fe/MgO sample genesis: (a) magnesium hydroxy-carbonate; (b) precursor; (c) reduced sample; light shading represents Fe^{3+}- or Fe^{2+}-rich regions; dark shading represents metallic iron.

reduction. Even for low metal loadings, due to this clustering, metallic iron can be formed, and in fact, the fraction of metallic iron in the reduced samples varies only slightly with metal loading.

ACKNOWLEDGMENTS

This work was supported by Grant No. GK 17451X of the National Science Foundation which also provided a Fellowship to one of us (J.A.D.). The help of the Center for Materials Research at Stanford University in X-ray diffraction and electron microscopy studies, and that of the Haldor Topsøe Research Laboratories in electron microscopy are gratefully acknowledged.

REFERENCES

1. Boudart, M., *in* "Advances in Catalysis" (D. D. Eley, H. Pines and P. B. Weisz, Eds.), Vol. **20,** p. 153. Academic Press, New York, 1969.
2. Boudart, M., Aldag, A. W., Benson, J. E., Dougharty, N. A., and Harkins, C. G., *J. Catal.* **6,** 92 (1966).
3. Emmett, P. H., and Brunauer, S., *J. Amer. Chem. Soc.* **59,** 1553 (1937).
4. Benson, J. E., and Boudart, M., *J. Catal.* **4,** 704 (1965).
5. Topsøe, H., Dumesic, J. A., and Boudart, M., *J. Catal.* **28,** 477 (1973).
6. Wiedersich, H., *in* "Proceedings of the Second Symposium on Low Energy X- and Gamma Sources," (P. S. Baker and M. Gerrard, Eds.). Austin, TX, 1967.
7. Shirane, G., Cox, D. E., and Ruby, S. L., *Phys. Rev.* **125,** 1158 (1962).
8. Bhide, V. G., and Tambe, B. R., *J. Mater. Sci.* **4,** 955 (1969).
9. Simkin, D. J., Ficalora, P. J., and Bernheim, R. A., *Phys. Lett.* **19,** 536 (1965).
10. Preston, R. S., Hanna, S. S., and Heberle, J., *Phys. Rev.* **128,** 2207 (1962).
11. Dumesic, J. A., Topsøe, H., and Boudart, M., *J. Catal.* **37,** 513 (1975).
12. Unpublished data.
13. Westerik, R., and Zwietering, P., *Proc. Kon. Ned. Akad. Wetensch. Ser. B* **56,** 492 (1953).
14. Warren, B. E., *J. Appl. Phys.* **12,** B75 (1941).
15. Jones, F. W., *Proc. Roy. Soc., Ser. A* **166,** 16 (1938).
16. Guilliatt, I. F., and Brett, N. H., *Trans. Brit. Ceram. Soc.* **69,** 1 (1970).
17. Anderson, P. J., *Mater. Res. Bull.* **3,** 537 (1968).
18. Dumesic, J. A., Topsøe, H., Anderson, J. H., and Boudart, M., *Surface Sci.,* in press (part V of this series).
19. Selwood, P. W., Adsorption and Collective Paramagnetism, Chap. 3. Academic Press, New York, 1962.
20. Ariya, S. M., Bobrysheva, N. P., Brach, B. Y., and Smirnova, G. A., *Sov. Phys. Solid State* **13,** 166 (1971).
21. Razouk, R. I., and Mikhail, R. S., *J. Phys. Chem.* **63,** 1050 (1959).
22. Guilliatt, I. F., and Brett, N. H., *Phil. Mag.* **21,** 671 (1970).
23. Dumesic, J. A., Topsøe, H., Khammouma, S., and Boudart, M., *J. Catal.* **37,** 503 (1975).
24. Luborsky, F. E., and Lawrence, P. E., *J. Appl. Phys.* **32,** 231S (1961).
25. Mulay, L. N., Collins, D. W., and Fisher, W., Jr., *Jap. J. Appl. Phys.* **6,** 1342 (1967).
26. McNab, T. K., PhD dissertation, Univ. of Western Australia, 1968.
27. Kündig, W., Bömmel, H., Constabaris, G., and Lindquist, R. H., *Phys. Rev.* **142,** 327 (1966).

28. Takei, H., and Chiba, S., *J. Phys. Soc. Jap.* **21,** 1255 (1966).
29. Coey, J. M. D., and Khaalafalla, D., *Phys. Status Solidi (A)* **11,** 229 (1972).
30. Large, N. R., Wilkinson, R. W., and Bullock, R. J., United Kingdom Atomic Energy Authority Research Group Report, AERE-R 5580, Chem. Division, Atomic Energy Research Establishment, Harwell, Berkshire, 1968.
31. Morrish, A. H., "The Physical Principles of Magnetism," p. 360. Wiley, New York, 1965.
32. Dumesic, J. A., Topsøe, H., and Boudart, M., *Surface Sci.,* in press (part IV of this series).
33. Ross, P. N., Jr., and Delgass, W. N., *Proc. Int. Congr. Catal., 5th, 1972,* p. 597 (1973).
34. Holm, V. C. F., and Clark, A., *J. Catal.* **11,** 305 (1968).
35. Yoshioka, T., Koezuka, J., and Ikoma, H., *J. Catal.* **16,** 264 (1970).
36. Murdoch, J., *Amer. Mineral.* **39,** 24 (1954).
37. Harrison, C. G. A., and Peterson, M. N. A., *Amer. Mineral.* **50,** 704 (1965).
38. Peacock, M. A., *Trans. Roy. Soc. Can., Sect. 4* **36,** 117 (1942).
39. Emmett, P. H., and Brunauer, S., *J. Amer. Chem. Soc.* **56,** 35 (1934).